Completely Buried, Non-Ion-Paired Glutamic Acid Contributes Favorably to the Conformational Stability of Pyrrolidone Carboxyl Peptidases from Hyperthermophiles[†,‡]

Jai K. Kaushik,[*,§,||] Satoshi Iimura,[||,⊥] Kyoko Ogasahara,[#] Yuriko Yamagata,[¶] Shin-ichi Segawa,[⊥] and Katsuhide Yutani[*,£]

Molecular Biology Unit, National Dairy Research Institute, Karnal 132001, India, School of Science and Technology, Kwansei Gakuin University, Sanda, Hyogo 669-1337, Japan, Institute for Protein Research, Osaka University, 3-2 Yamadaoka, Suita, Osaka 565-0871, Japan, Graduate School of Pharmaceutical Sciences, Kumamoto University, 5-1 Oe-honmachi, Kumamoto 862-0973, Japan, and RIKEN SPring-8, Harima Institute, 1-1-1 Kouto, Sayo, Hyogo 679-5148, Japan

Received December 22, 2005; Revised Manuscript Received April 18, 2006

ABSTRACT: Pyrrolidone carboxyl peptidases (PCPs) from hyperthermophiles have a structurally conserved and completely buried Glu192 in the hydrophobic core; in contrast, the corresponding residue in the mesophile protein is a hydrophobic residue, Ile. Does the buried ionizable residue contribute to stabilization or destabilization of hyperthermophile PCPs? To elucidate the role of the buried glutamic acid in stabilizing PCP from hyperthermophiles, we constructed five Glu192 mutants of PCP-0SH (C142S/C188S, Cys-free double mutant of PCP) from *Pyrococcus furiosus* and examined their thermal and pH-induced unfolding and crystal structures and compared them with those of PCP-0SH. The stabilities of apolar (E192A/I/V) and polar (E192D/Q) mutants were less than PCP-0SH at acidic pH values. In the alkaline region, the mutant proteins, except for E192D, were more stable than PCP-0SH. The thermal stability data and theoretical calculations indicated an apparent pK_a value ≥7.3 for Glu192. Present results confirmed that the protonated Glu192 in PCP-0SH forms strong hydrogen bonds with the carbonyl oxygen and peptide nitrogen of Pro168. New intermolecular hydrogen bonds in the E → A/D mutants were formed by a water molecule introduced into the cavity created around position 192, whereas the hydrogen bonds disappeared in the E → I/V mutants. Structure-based empirical stability of mutant proteins was in good agreement with the experimental results. The results indicated that (1) completely buried Glu192 contributes to the stabilization of PCP-0SH because of the formation of strong intramolecular hydrogen bonds and (2) the hydrogen bonds by the nonionized and buried Glu can contribute more than the burial of hydrophobic groups to the conformational stability of proteins.

In the past decade, crystal structures of proteins from extremophiles have appeared at an increasing rate. The accumulated structures provide useful insight into understanding the origin for enhanced thermostability of hyperthermophile proteins (*1*, *2*). However, the origin of very high stability does not arise from a single mechanism or structural feature but rather depends upon several factors such as increased salt bridges, improved hydrogen bonding, favorable packing interactions, fewer cavities, improved hydrophobic interactions, secondary-structure stability, higher oligomerization, or their combination (*1*−*6*). On the other hand, it has been debated whether structural features directly relate to the enhanced stability for hyperthermophilic proteins (*7*). There are some controversial views regarding the contribution of some important factors to protein stability. Salt bridges have been known to have negative (*8*, *9*) as well as positive contributions (*5*, *6*, *10*−*12*) in the conformational stability of proteins. Similarly, despite the reports of a negligible or negative contribution (*8*, *15*, *16*) of hydrogen bonds to protein stability, an increasing number of studies (*3*, *4*, *13*, *14*, *17*−*25*) have indicated the important role of hydrogen bonding to the thermal stability of proteins. Therefore, to determine the factors responsible for the ultrahigh stability of hyperthermophilic proteins, it is important to verify whether some unique structural features of hyperthermophilic proteins contribute to their stability by analysis of the relationship between structure and stability using mutant proteins.

[†] This work was supported in part by a Grant-in-Aid for special project research and the "National Project for Protein Structural and Functional Analysis" funded by the Ministry of Education, Culture, Sports, Science, and Technology of Japan (to Y.Y. and K.Y.) and a JSPS Fellowship (to J.K.K.).

[‡] The final coordinates of the PCP-0SH mutants have been deposited in the Protein Data Bank. The accession codes are 1X10, 1X12, 1Z8W, 1Z8T, and 1Z8X for E192A, E192D, E192I, E192Q, and E192V, respectively.

* To whom correspondence should be addressed: RIKEN SPring-8 Center, Harima Institute, 1-1-1 Kouto, Sayo-cho, Sayo-gun, Hyogo 679-5148, Japan. Telephone: 81-791-58-2937. Fax: 81-791-58-2917. E-mail: yutani@spring8.or.jp (K.Y.); National Dairy Research Institute, Karnal 132001, India. E-mail: jai@ndri.res.in (J.K.K.).

[§] National Dairy Research Institute.

[||] These authors contributed equally.

[⊥] Kwansei Gakuin University.

[#] Osaka University.

[¶] Kumamoto University.

[£] RIKEN Harima Institute.

10.1021/bi052610n CCC: $33.50
Published on Web 05/20/2006

Crystal structures of pyrrolidone carboxyl peptidase (PCP)[1] from *Pyrococcus furiosus*, *Pf*PCP, and its Cys-free (C142S/C188S) form, PCP-0SH (*26*), *Thermococcus litoralis*, *Tl*PCP (*27*), *Pyrococcus horikoshii*, *Ph*PCP (*28*), and mesophile *Bacillus amyloliquefaciens*, *Ba*PCP (*29*), have been determined. On the basis of crystal structure analyses of *Pf*PCP and PCP-0SH and *Tl*PCP compared to *Ba*PCP, it has been indicated that the higher stability of *Pf*PCP is caused by increases in the hydrophobic interactions and hydrogen bonds, the formation of an intersubunit ion-pair network, and improvement to an ideal conformation and concluded that the conformational structures of *Pf*PCP and PCP-0SH are superior in their combination of positive- and negative-stabilizing factors compared to *Ba*PCP (*26*). PCP-0SH is a homotetramer, and its monomer consists of 208 residues (MW = 22 800). Its oligomerization state changes to dimer and monomer depending upon pH and the thermal, and chemical denaturation of the monomeric and dimeric forms is reversible (*30*, *31*). The thermodynamic and kinetic stabilities of *Pf*PCP and PCP-0SH have been studied in detail (*31*−*33*).

A unique structural feature of the three PCPs from the hyperthermophiles is the existence of a Glu residue completely buried in the hydrophobic pocket without any salt-bridge-forming partner in the vicinity (*26*). The sequence and structure alignment of *Pf*PCP, *Tl*PCP, and *Ph*PCP with the mesophilic *Ba*PCP indicate that a glutamic acid (E192 in *Pf*PCP, E194 in *Tl*PCP, and E185 in *Ph*PCP) is conserved among the hyperthermophiles, while *Ba*PCP has Ile189 at the corresponding position. Buried noncharged polar groups lacking a hydrogen-bond partner are very destabilizing and incur an energy penalty up to 12.5 kJ/mol (*34*). It seems to suggest that a buried ionizable group lacking a salt-bridge partner in the hyperthermophile proteins should incur much higher energetic penalty; in contrast, Ile189 in *Ba*PCP should have a hydrophobic-stabilizing effect. Then, the replacement of E192 by a hydrophobic residue might be expected to increase the stability of the mutant protein of *Pf*PCP.

In this study, to understand the seemingly unusual location of the conserved Glu residue among PCPs from hyperthermophiles, we replaced glutamic acid at position 192 in PCP-0SH with apolar (Ile, Ala, and Val) and polar (Gln and Asp) residues. We determined the thermal and pH stability and also the crystal structures by the X-ray diffraction analyses of the mutant proteins and compared them to those of PCP-0SH. The obtained physicochemical results were highly unexpected; that is, PCP-0SH was more stable than all of the mutant proteins at low pH, indicating that the buried Glu in hyperthermophiles is important for their higher stability. On the other hand, the E → D mutant was more stable than the highly apolar mutants such as E → I and E → V as well as polar mutant E → Q at low pH but more unstable with respect to all of the other mutant proteins at neutral and alkaline pH zones. We will discuss the mechanism by which the buried Glu in hyperthermophile PCPs contribute to the stabilization based on the crystal structural features of each of the mutant proteins of PCP-0SH.

[1] Abbreviations: PCP, pyrrolidone carboxyl peptidase; PCP-0SH, pyrrolidone carboxyl peptidase without cysteines (C142S/C188S) from *Pyrococcus furiosus*; DSC, differential scanning calorimetry; CD, circular dichroism; GdmCl, guanidinium chloride; T_d, peak temperature on the DSC endotherm in a thermal transition; $\Delta T_d = T_d^{mutant} - T_d^{PCP-0SH}$, difference in T_d values of a mutant and PCP-0SH; rms, root-mean-square; $\Delta G_u^{\ddagger H_2O}$, Gibbs energy of activation in an unfolding reaction from a native state, *N*, to a transition state, $T^{\ddagger}$.

EXPERIMENTAL PROCEDURES

Construction, Expression, and Purification of Mutant Proteins. The mutants E192A, E192D, E192I, E192Q, and E192V of the PCP-0SH, which is the Cys-free mutant of PCP from *P. furiosus*, were constructed by site-directed mutagenesis, expressed in *Escherichia coli*, and purified as previously described (*30*). The buffers used were Gly-HCl (pH 1.57−3.04), potassium phosphate (pH 7.3), or Gly-KOH (pH 8.6−9.6) at a concentration of 20 mM. The protein concentration was determined using an absorption coefficient of $E^{1\%}_{1\ cm} = 6.6$ at 278.5 nm (*31*). Guanidinium chloride (GdmCl) (special grade) from Nacalai Tesque (Japan) was used. All of the chemical reagents used were of analytical grade.

Measurement of the Thermal Stability of Proteins. The thermal denaturation of the proteins was measured using a VP-DSC (Microcal LLC, Northampton, MA) or Nano-DSC II 6100 (CSC, Inc., Portland, OR) microcalorimeters as previously described (*30*, *32*). Proteins samples were dialyzed for 20 h against 20 mM Gly-HCl (pH 2.15 and 3.04) or 20 mM Gly-KOH (pH 9.6) by submerging all of the dialysis tubes containing proteins in the same vessel with buffer to maintain the similar pH for all of the mutant proteins. The buffer was replaced with a fresh lot once after 4 h from the beginning. For the differential scanning calorimetry (DSC) measurements of the proteins in the presence of GdmCl, the proteins were dissolved in 2.5 M GdmCl solution, filtered through a membrane with 10 kDa cutoff pore size, and then washed several times with 2.5 M GdmCl solution to equilibrate (*35*).

Measurement of Unfolding Rates of Proteins. The unfolding rate of proteins was measured by the GdmCl concentration jump and monitoring the protein denaturation by a change in the ellipticity at 222 nm on a Jasco-720 spectropolarimeter as described earlier (*31*). The progress curves were analyzed by the least-squares method to determine the rate constant using eq 1

$$Y(t) = Y_o + \sum A_i e^{-k_i t} \quad (1)$$

where Y is the signal at any time (t), Y_o is the signal value when no further change is observed, k_i is the apparent rate constant, and A_i is the total amplitude of the ith kinetic phase. The unfolding rate in water, $k_u^{H_2O}$, for various proteins was calculated by linear least-squares fitting of $\log[k_u]$ versus the GdmCl concentration [C] plots according to eq 2

$$\log k_u = \log k_u^{H_2O} + m[C] \quad (2)$$

The activation Gibbs energy change for $N \rightarrow T^{\ddagger}$ conversion, where N is the native state and $T^{\ddagger}$ denotes the transition state in an unfolding reaction, was determined according to the transition-state theory using the Eyring equation as given below

$$\Delta G_u^{\ddagger(H_2O)} = RT \ln[k_B T/h k_u^{H_2O}] \quad (3)$$

where k_B is Boltzmann's constant, h is Planck's constant, R

is the gas constant, and T is the temperature in Kelvin. The changes in the unfolding Gibbs energy of activation in water, $\Delta\Delta G_u^{\ddagger(H_2O)}$ was calculated by taking the difference between the activation Gibbs energy of unfolding of the mutant proteins and the wild-type protein.

Measurement of pH-Induced Protein Stability. pH titration curves in the acidic region were monitored from the circular dichroism (CD) values at 222 nm. Prior to the CD measurement, the protein samples were dialyzed against 20 mM Gly buffer at pH 1.57 and thermally denatured at 60−62 °C for 12 min, followed by cooling and adjusting the pH to various values by adding KOH. The solutions were incubated for 1 week at 30 °C to attain equilibrium of the refolding reaction as determined earlier (*32*).

Crystallization and X-ray Data Collection. An 1.5 μL aliquot of PCP-0SH and each of the E192 mutants of PCP-0SH at a concentration of around 4−6 mg/mL in 50 mM Na-acetate buffer at pH 4.6 was mixed with an equal volume of reservoir solution (50 mM Na-acetate buffer at pH 4.6, including PEG4000 at various concentrations). Crystals suitable for data collection were obtained using the hanging-drop vapor diffusion method at room temperature. X-ray diffraction data for all of the mutants, except for E192Q, were collected at the SPring8 BL-40B2 and BL-41XU synchrotron beamlines equipped with area detectors, while data for E192Q were collected at BL-6A beamline equipped with a Weissenberg camera at Photon Factory, Tsukuba, Japan. The protein crystals were soaked in 25−30% glycerol before data collection at 100 K using flash cooling. The intensity data were processed using the HKL program suite (*36*).

Structure Solution and Refinement. The structures of the E192 mutants of PCP-0SH were solved by the molecular-replacement method, employing the AMoRe program package (*37*) using the coordinates of PCP-0SH (PDB ID 1IOI) as a template structure. The protein structure was refined using CNS (*38*) and graphical interface "O" (*39*). One molecule was built into the electron-density map in program "O", and the other molecules in the asymmetric unit were generated by the NCS operation. The quality of the models was inspected by ProCheck (*40*).

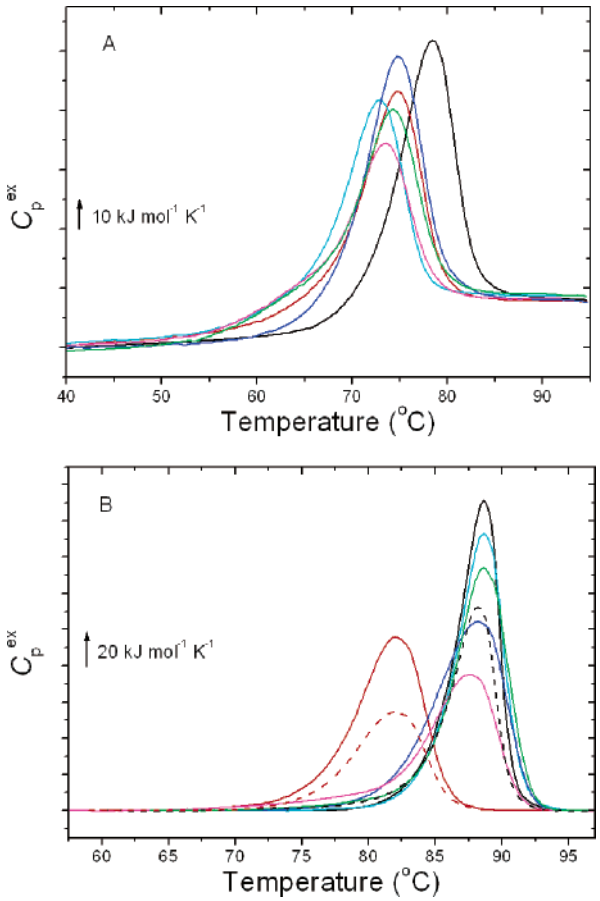

FIGURE 1: Typical excess-heat-capacity (DSC) curves for denaturation of PCP-0SH and E192 mutants at a scan rate of 1 °C/min. All of the curves have been corrected for the corresponding buffer baselines. The curves are PCP-0SH (black), E192D (red), E192Q (cyan), E192A (blue), E192I (green), and E192V (magenta). (A) DSC curves at pH 3.04 and (B) DSC curves at pH 7.3 (in the presence of 2.5 M GdmCl). The dashed lines are excess-heat-capacity curves over reheating the sample cooled to 25 °C after the first scan. For clarity, only PCP-0SH (black dashed line) and E192D (red dashed line) reversibility curves have been shown; other mutant proteins also showed reversible denaturation in the presence of GdmCl. All of the curves at pH 7.3 have been subtracted with a progressive baseline between the native and denatured states.

RESULTS

Stability of PCP-0SH and Glu192 Mutants. Thermal stabilities of the PCP-0SH and E192 mutant proteins were measured at various pH values using DSC at a scan rate of 1 °C/min (Figure 1). In the acidic region, the DSC curves of the PCP-0SH (*32*) and E192 mutants were completely reversible; in contrast, at higher pH values, the denaturation of all of the proteins became irreversible. However, inclusion of 2.5 M GdmCl in the protein solution at neutral and higher pH values restored the partial reversibility as estimated by recovery of the enthalpy of denaturation over reheating the protein solution. No aggregation was observed in the presence of GdmCl at higher pH values or at acidic pH even without GdmCl, as revealed by the absence of any abrupt change in the excess-heat-capacity curves of proteins (Figure 1). Addition of GdmCl not only decreased the denaturation temperature but also helped in increasing the protein solubility.

At low pH, the denaturation reactions were reversible but did not attain equilibrium because of the unusually slow denaturation rate of the PCP-0SH (*32*). The peak temperatures on the DSC curves of the E192 mutants were also scan-rate-dependent at all of the pH values with or without GdmCl. Therefore, the data were not amenable to rigorous thermodynamic analyses because of nonequilibrium conditions. Therefore, the change in the stability of the mutant proteins as a result of substitution was estimated from the peak temperature (T_d) on the DSC curves. The DSC results shown in Table 1 indicate that substitution of E192 has a significant effect on the stability of PCP-0SH and the change in stability varied depending upon the residues at position 192. The T_d value for all of the proteins increased with increasing pH (Table 1). The T_d values of PCP-0SH are consistent with those reported earlier at various pH values (*30*). At pH 2.15, E192V did not show a thermal transition, indicating that the protein might already be denatured. The T_d values at pH 2.15 for various proteins increased in the order of E192I, E192Q, E192A, E192D, and PCP-0SH. The E192D was the most stable among the mutant proteins. Figure 2 shows the change in the relative stability (ΔT_d =

Table 1: Comparison of Stabilities of PCP-0SH and Its Mutants at Various pH Values

	T_d values (°C)[a]					
pH[b]	PCP-0SH	E192A	E192D	E192I	E192Q	E192V
2.15	59.3	54.5	55.2	52.8	53.4	
3.04	78.9	74.6	74.8	74.1	72.6	73.3
7.30[c]	88.6	88.3	82.1	88.6	88.6	87.6
8.70[c]	88.8	89.4	82.0	90.2	89.3	88.9
9.60[d]	101.7	103.1	98.0	102.6	102.6	103.6

[a] T_d represents peak temperatures of DSC curves monitored at a scan rate of 1 °C/min. The given values are an average of independent scans 3−5 times. The repeatability of T_d values for a given protein was within 0.25 °C in cases of reversible denaturation in the pH region between 2.15 and 8.70. [b] pH was measured before and after the heating. The maximum difference in the pH values was 0.03. The indicated pH values are an average of the values before and after the heating. [c] A total of 2.5 M GdmCl was added in solutions at pH 7.3 and 8.7. [d] Partial aggregation was observed at pH 9.6 after heating beyond 100 °C.

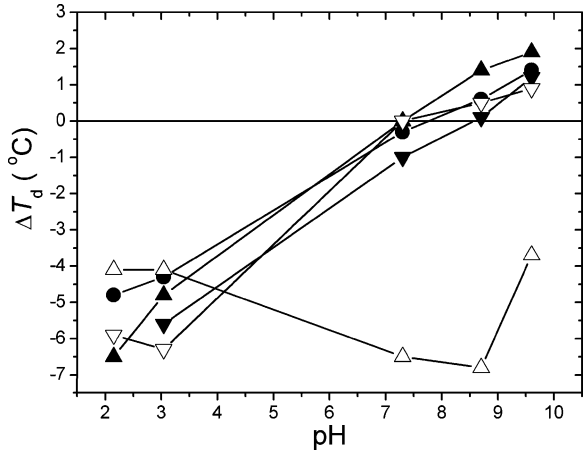

FIGURE 2: Relative stability ($\Delta T_d = T_d^{mutant} - T_d^{PCP-0SH}$) of E192 mutants of PCP-0SH as a function of pH. The T_d values at pH 7.3 and 8.6 were measured in the presence of 2.5 M GdmCl. The symbols represent E192A (●), E192D (△), E192I (▲), E192Q (▽), and E192V (▼).

$T_d^{mutant} - T_d^{PCP-0SH}$) of the E192 mutant proteins compared to PCP-0SH as a function of pH. All of the mutant proteins were less stable than PCP-0SH up to pH 7.3. In the alkaline region, the stability of the mutants, except for E192D, became equal or higher than PCP-0SH. E192D was the most unstable among the mutants of PCP-0SH in the neutral and alkaline regions.

The kinetics of GdmCl-mediated denaturation indicated that PCP-0SH and E192 mutants have extremely slow unfolding rates. The unfolding reaction could not be measured within the perceptible time frame at 30 °C at neutral and alkaline regions because of extremely slow unfolding rates on the order of 10^{-15} s^{-1} (*31*); therefore, unfolding kinetics was measured at 60 °C at pHs 7.0 and 10.5. Results shown in Table 2 indicate that substitution of E192 leads to an increase in the unfolding rate of up to 2 orders of magnitude at pH 2.4. The change in the Gibbs energy of activation ($\Delta\Delta G_u^{\ddagger H_2O}$) of the mutant proteins relative to PCP-0SH showed that E192D and E192A are kinetically more stable than other mutants at pH 2.4, which is consistent with the ΔT_d values at low pH (Figure 2). At neutral pH, the value of $\Delta G_u^{\ddagger H_2O}$ for PCP-0SH is only marginally higher than that for other mutant proteins. On the other hand, at pH 10.5,

Table 2: Kinetic Parameters of the Denaturation of PCP-0SH and E192 Mutants at Various pH Values

protein	$k_u^{H_2O}$ (s^{-1})	$\Delta G_u^{\ddagger H_2O}$ (kJ mol^{-1})	$\Delta\Delta G_u^{\ddagger H_2O}$ [a,b] (kJ mol^{-1})
pH 2.4, Temperature 30 °C			
PCP-0SH	1.17×10^{-7}	114.5	0.0
E192D	8.32×10^{-7}	109.5	−5.0
E192Q	1.55×10^{-6}	108.0	−6.5
E192A	1.00×10^{-6}	109.1	−5.4
E192I	1.51×10^{-6}	108.0	−6.5
E192V	6.92×10^{-6}	104.2	−10.3
pH 7.0, Temperature 60 °C			
PCP-0SH	2.00×10^{-9}	137.4	0.0
E192D	1.00×10^{-8}	132.9	−4.5
E192Q	4.07×10^{-9}	135.4	−2.0
E192A	4.19×10^{-9}	135.3	−2.1
E192I	4.30×10^{-9}	135.1	−2.3
E192V	5.01×10^{-9}	134.8	−2.6
pH 10.5, Temperature 60 °C			
PCP-0SH	7.50×10^{-8}	127.3	0.0
E192D	6.92×10^{-8}	127.5	0.2
E192Q	1.79×10^{-8}	131.2	3.9
E192A	1.26×10^{-8}	132.2	4.9
E192I	2.51×10^{-8}	130.3	3.0
E192V	1.32×10^{-8}	132.1	4.8

[a] $\Delta\Delta G_u^{\ddagger H_2O} = \Delta G_u^{\ddagger H_2O(mut)} - \Delta G_u^{\ddagger H_2O(PCP-0SH)}$. [b] The positive values of $\Delta\Delta G_u^{\ddagger H_2O}$ mean that mutant proteins are more stable than the wild type.

PCP-0SH and E192D showed similar Gibbs energy of activation, while all other mutants were kinetically more stable than PCP-0SH. These results are in very good agreement with the thermal stability data obtained by DSC at various pH values, suggesting that the change in stability because of E192 substitution might be originating from the alteration in the unfolding Gibbs energy of activation. PCP-0SH unfolds with an extremely slow rate, on the order of 10^{-15} s^{-1} (relaxation time ∼ 20 million years) at neutral pH, whereas the mesophilic *Ba*PCP unfolds with a rate of 10^{-8} s^{-1} (*31*). On the other hand, both the proteins showed similar refolding rates on the order of 0.1 s^{-1} at neutral pH, despite only ∼40% amino acid sequence identity. A comparison of the relaxation kinetics of several mesophilic and hyperthermophilic proteins indicated that refolding rates were conserved, while the unfolding rates differed significantly between them (*41*). Because of the conserved refolding rates, the difference in the unfolding rate should result in a net change in the stability of the mutant protein. In the absence of thermodynamic parameters under equilibrium conditions, therefore, the change in the stability of the mutant protein can be reliably estimated from the change in the T_d or $\Delta G_u^{\ddagger H_2O}$ values with respect to PCP-0SH.

pH Stability of PCP-0SH and Mutant Proteins. Figure 3 shows the equilibrium curves for the refolding reactions monitored from CD values at 222 nm, which are equivalent to the equilibrium denaturation curves, for the proteins as a function of pH. PCP-0SH was the most stable with a pH_{50} at 1.79 ± 0.04, where pH_{50} is the pH value corresponding to 50% renaturation of the protein. The pH_{50} values for the mutant proteins were observed to be 2.12 ± 0.04 for E192D, 2.16 ± 0.03 for E192A, 2.35 ± 0.03 for E192Q and E192I, and 2.37 ± 0.04 for E192V. The decrease in the pH stability of the E192 mutant proteins was in very good agreement

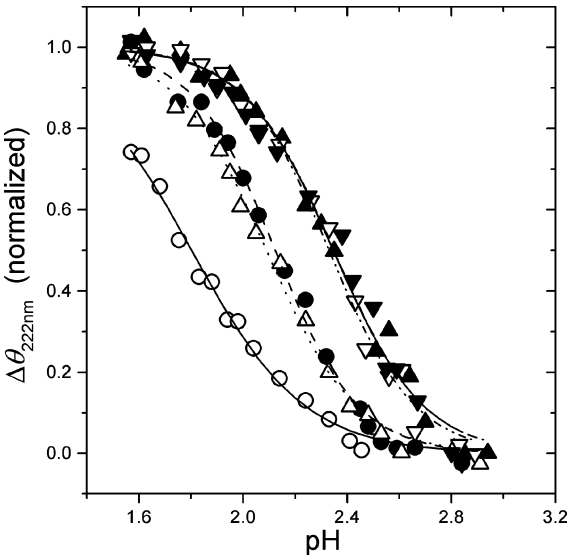

FIGURE 3: pH stability of PCP-0SH and E192 mutants. The pH stability curves are equivalent to the equilibrium denaturation curves, which were monitored by the recovery of the CD values at 222 nm during the refolding reaction of the completely thermally denatured proteins at pH 1.57 as described in the text. Sigmoidal fitting curves were plotted to estimate the pH_{50} values. The fitting error was <0.01 pH unit, except for E192V, for which it was ~0.02. The open circle indicates the PCP-0SH, and the other symbols for the mutant proteins are the same as used in Figure 2.

with the order of the thermal stability obtained by DSC measurements at low pH. This implies that the results obtained by DSC, which are kinetic in nature because of scan-rate dependence of T_d values, can be directly related to the equilibrium results at acidic pH values. The values of ΔH_d (not shown) for the mutant proteins obtained from the area under excess-heat-capacity curves obtained by DSC were much lower than that of PCP-0SH at pH 2.15. This can be explained by pH_{50} values; even the most stable mutant E192D was already denatured by 50% at pH 2.15, while PCP-0SH was denatured by only ~20%. The fractional denaturation of E192V at pH 2.15 was about 73%, which explains the absence of the endotherm in the case of E192V at pH 2.15 during the heat denaturation.

Crystallization and Structure Analysis of Glu192 Mutants. The PCP-0SH polar mutants (E192D/Q) crystallized at a 6.5% PEG4000, while the apolar mutants (E192A/I/V) crystallized at a 5.7−6.0% PEG4000. The final R_{free} for the mutant proteins was obtained between 20 and 25%. The statistics of the data collection and structure refinement are shown in Tables 3 and 4, respectively.

The protein molecules crystallized in two different space groups. E192Q and E192V formed isomorphic monoclinic crystals in the space group $P2_1$, which agree with those of the wild-type PCP and PCP-0SH (*26*), while E192A, E192D, and E192I formed orthorhombic crystals in the space group $P2_12_12_1$. In both crystal systems, four subunit (monomer) molecules were contained in the asymmetric unit.

A systematic analysis of individual structures indicated that the mutation did not have any significant effect on the overall structure as revealed by a very good least-squares superimposition of their backbone atoms. The root-mean-square (rms) deviations for the backbone atoms between PCP-0SH and the mutant proteins were observed below 0.2 Å. It was on the lower side (0.14 ± 0.01 Å) for the molecules in the $P2_1$ space group (same for PCP-0SH) as compared to those in the $P2_12_12_1$ space group (0.2 ± 0.01 Å). Overall, the structure of PCP-0SH was not significantly affected by the mutations. The differences in the surface details could be due to different crystal packing.

Structure of PCP-0SH near Glu192. The PCP-0SH structure has been determined previously at 2.7 Å at room temperature (*26*). In this study, we again solved its structure at 2.1 Å and 100 K. All of the calculations were carried out using the new structure, which was essentially similar to the previous one. In the PCP-0SH structure, the carbonyl O atom of P168 is located at a distance of 2.56 Å from the $O^{\epsilon 2}$ atom of E192 (Figure 4A). This indicates that E192 in the protonated state might form a strong hydrogen bond, O(P168)···H−$O^{\epsilon 2}$ (E192). The angles AA−A−D and DD−D−A and the dihedral angle AA−A−D−DD are observed around 119°, 128°, and 171°, respectively, where D is the hydrogen donor, DD is the atom covalently connected to D, A is the acceptor, and AA is the atom covalently connected to A. The observed (P168)−O···$O^{\epsilon 2}$−(E192) distance and angles were close to the optimal values for making a good hydrogen bond (*42*). The peptide nitrogen in P168 located at 3.32 Å from E192 $O^{\epsilon 2}$ with a DD−D−A angle of 131.9° can also form a bifurcate intramolecular hydrogen bond by sharing the proton of E192 $O^{\epsilon 2}$. The E192 $O^{\epsilon 1}$ atom does not form any hydrogen bond because of lack of a donor group in the vicinity. The average *B* factor for the E192 residue was observed to be 23.3 ± 1.3 $Å^2$ (averaged for Glu in four subunits), which is considerably lower than the average *B* factor of the PCP-0SH molecule (30.1 ± 1.2 $Å^2$), indicating that Glu at position 192 is highly ordered in the hydrophobic pocket because of strong interactions.

Glu192 → Gln(E192Q). In E192Q, the Gln $N^{\epsilon 2}$ atom is located close to the carbonyl O atoms of P168 (3.01 Å) and M187 (3.05 Å) as shown by arrows in Figure 4B. The AA−A−D/DD−D−A angles formed by Gln $N^{\epsilon 2}$ and carboxyl O atoms of P168 (123.9°/117.6°) and M187 (131.1°/125.8°) were optimal values for forming ideal hydrogen bonds. The Q192 $O^{\epsilon 1}$ atom is not involved in any hydrogen-bond interaction because of lack of a donor group in the vicinity. The *B* factor for Q192(residue)/E192Q(subunit) was observed to be 19.3 ± 1.2/25.8 ± 0.6 $Å^2$ (averaged for the subunits). The rms deviations between PCP-0SH and E192Q for the backbone atoms (C_α) of the monomer and for residues in the vicinity of position 192 in the pocket (residues P18/168, I22/76, Y169, M187, S188, E192, A195, and V196) were 0.13 and 0.08 Å, respectively, suggesting no significant difference in their overall and local structures around position 192.

Glu192 → Asp (E192D) and Glu192 → Ala (E192A). The substitution of E192 by Asp and Ala with smaller side chains led to the formation of a cavity in which a water molecule is introduced in the hydrophobic pocket (parts C and D of Figure 4). In both mutant proteins, a water molecule is located close to P168 and in a corresponding position occupied by the $O^{\epsilon 2}$ atom of E192 in PCP-0SH, suggesting the possibility that a water molecule forms new intermolecular hydrogen bonds in place of the intramolecular hydrogen bonds formed by E192 in PCP-0SH.

In E192D (Figure 4C), a water molecule is located at a distance of 2.55 Å from the $O^{\epsilon 2}$ atom of D192 and 2.63 Å

Table 3: X-ray Data Collection Statistics for PCP-0SH and Glu192 Mutants

	PCP-0SH	E192A	E192D	E192I	E192Q	E192V
space group	$P2_1$	$P2_12_12_1$	$P2_12_12_1$	$P2_12_12_1$	$P2_1$	$P2_1$
cell dimensions						
a (Å)	55.56	47.44	47.45	47.41	56.17	56.55
b (Å)	104.58	103.96	103.85	103.92	104.91	104.54
c (Å)	79.16	187.49	187.06	186.39	79.23	77.36
β (deg)	91.78	90.00	90.00	90.00	91.84	92.80
resolution range (Å)	50.0−2.1	50.0−2.0	50.0−2.0	50.0−2.0	40.0−2.4	50.0−2.0
number of measured reflections	195 727	316 205	304 598	311 999	100 815	212 213
number of unique reflections	53 620	62 100	62 491	60 478	32 566	59 076
redundancy	3.7	5.1	4.9	5.2	3.1	3.6
completeness (%)	99.1 (84.1)[a]	97.9 (96.9)	97.9 (96.9)	95.0 (69.8)	90.6 (78.9)	96.2 (73.1)
$I/\sigma(I)$	28.2 (10.8)	30.7 (15.2)	38.7 (23.7)	36.8 (19.4)	17.5 (4.1)	30.3 (16.7)
R_{merge}[b] (%)	5.4 (13.6)	4.8 (8.3)	2.7 (4.4)	4.1 (7.7)	5.4 (12.6)	4.1 (6.9)

[a] Values in parentheses refer to the highest resolution shell. [b] $R_{merge} = \sum|I_{hkl} - \langle I_{hkl}\rangle|/\sum I_{hkl}$, where $\langle I_{hkl}\rangle$ is the mean value of I_{hkl}.

Table 4: Structure Refinement Statistics for PCP-0SH and Glu192 Mutants

	PCP-0SH	E192A	E192D	E192I	E192Q	E192V
resolution range (Å)	40.0−2.1	50.0−2.0	40.0−2.0	40.0−2.0	40.0−2.5	50.0−2.0
number of protein atoms	6420	6404	6416	6416	6420	6412
number of water atoms	531	893	867	851	533	549
number of reflections	52 444	61 801	62 292	60 239	25 637	58 594
working set	49 800	58 682	59 150	57 201	24 380	55 624
test set (5% of total)	2644	3119	3142	3038	1257	2968
completeness (%)	99.4	97.0	98.1	95.2	81.2	96.6
R factor (%) ($>2\sigma F$)						
working set	20.6	20.6	17.9	18.0	20.4	20.9
test set	24.4	22.9	21.7	21.8	24.1	23.6
rmsd from ideality						
bond lengths (Å)	0.006	0.005	0.008	0.007	0.006	0.005
angles (deg)	1.29	1.26	1.38	1.34	1.25	1.25
Ramachandran plot (residues in)						
most favorable regions (%)	92.5	93.1	92.9	93.5	92.9	91.9
additional allowed regions (%)	7.5	6.9	7.1	6.5	7.1	8.1

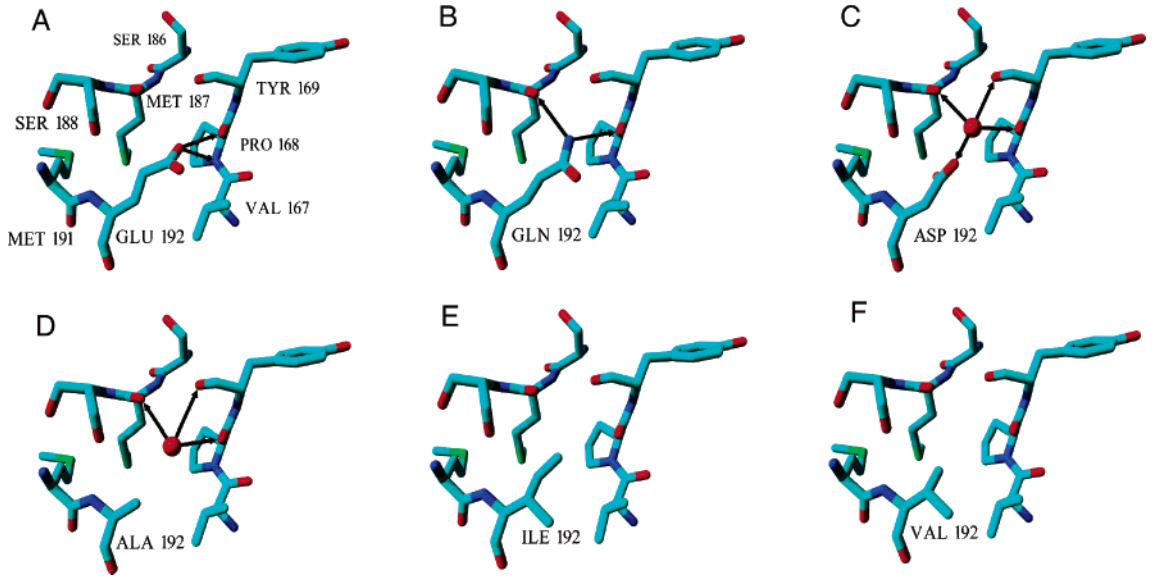

FIGURE 4: X-ray crystal structures of PCP-0SH and E192 mutant proteins around position 192. (A) PCP-0SH, (B) E192Q, (C) E192D, (D) E192A, (E) E192I, and (F) E192V. The solid red spheres in the E192D and E192A mutant proteins represent a water molecule found in the cavities. The solid arrows indicate the atoms within the hydrogen-bond-forming distance (D::A distances are given in the Results). Figures were produced using the Yasara-View program (www.yasara.org, Yasara Biosciences, Austria) and rendered by Pov-Ray version 3.6.

from the carbonyl O of P168, suggesting that the water molecule might form a bridge between D192 and P168 via hydrogen bonding. The carbonyl O atoms of Y169 and M187 are also located within the hydrogen-bond-forming distances of 3.08 and 2.79 Å, respectively, from the entrapped water molecule. The E → D mutation led to the cavity formation of ~13.5 Å^3 close to position 192 and a C_α rms deviation of 0.2 Å for the residues in the cavity.

In E192A (Figure 4D), the water molecule is located at a distance of 2.86, 2.95, and 3.58 Å from the carbonyl O atoms

of P168, M187, and Y169, respectively. The cavity introduced because of the E → A mutation was larger (24 Å^3) than that of D192; however, the C_α rms deviation of residues in the pocket was only 0.09 Å, suggesting a smaller change in the overall structure around the mutation site. The *B* factors for position 192 in the E192D and E192A were much lower at 9.6 ± 0.3 and 11.1 ± 0.5 Å^2, respectively. In both structures, the water molecules close to P168 were completely solvent-inaccessible and highly ordered (*B* factor ∼ 6.7−14 Å^2).

Glu192 → Ile (E192I) and Glu192 → Val (E192V). Substitution of Glu192 with Ile or Val resulted in the loss of intramolecular hydrogen bonds formed in PCP-0SH and E192Q or intermolecular protein−water hydrogen bonds in the E192A and E192D mutants, because E192I and E192V do not contain any water molecule close to the mutation site (parts E and F of Figure 4). Cavities with sizes of ∼26 and 28 Å^3 because of E → I and E → V replacements, respectively, were observed close to position 192. The C_α rms deviations between the structure of PCP-0SH and those of E192I and E192V were observed to be 0.2 and 0.15 Å, respectively, for the subunit, and 0.12 and 0.1 Å, respectively, for the residues in the vicinity of the mutation site. The *B*-factor values for the I192 residue/E192I subunit (12.7 ± 0.6/15.4 ± 1.2 Å^2) and the V192 residue/E192V subunit (24.0 ± 0.6/30.0 ± 1.0 Å^2) were lower than or close to those for PCP-0SH.

Overall, large shifts in the main chain, change in the secondary structure, or exposure of the buried groups around position 192 in PCP-0SH were not observed because of replacement of E192 as evident from the small C_α rms deviations and relatively unchanged positions of groups close to position 192 (Figure 4).

Structure-Based Empirical Stability of Mutant Proteins. Structures of the PCP-0SH and mutant proteins clearly indicate that deletions of hydrogen bonds formed by the residues at position 192 or by water with the neighboring residues lead to the decrease in the protein stability (T_d). On the other hand, because the residue 192 is completely buried, the substitutions by hydrophobic residues (Ile and Val) were also expected to stabilize the mutant protein. Therefore, it becomes difficult to discern the net effect of mutation on the stabilizing factors by the only observation of the structures. "Structure-based empirical stability" methods based on the experimentally measured stabilities and high-resolution structures of mutant proteins (*21*, *43*) can be a valuable tool to quantitatively estimate the changes in the stabilizing factors because of mutations.

The mutation leads to the addition or removal of some interactions, which leads to stabilization or destabilization of the protein structure. The change in stability because of mutations can be evaluated from the changes in the contributing components such as the hydrophobic effect ($\Delta\Delta G_{HP}$) and side-chain conformational entropy ($\Delta\Delta G_{conf}$) because of dissimilar sizes of the side chains of residues, hydrogen bonds ($\Delta\Delta G_{HB}$) because of the addition or deletion by new residue, entropic loss because of the addition or removal of internal water molecules ($\Delta\Delta G_{H_2O}$) in the cavities, cavity volume ($\Delta\Delta G_{cav}$), and the secondary-structural propensity of amino acid residues for the formation of α helix and β strand ($\Delta\Delta G_{pro}{}^{\alpha}$ and $\Delta\Delta G_{pro}{}^{\beta}$, respectively). Assuming that the structural changes because of substitutions are negligible in the region except for the mutation site, the stability difference because of the mutation can be represented by the following equation (*21*, *43*):

$$\Delta\Delta G = \Delta G^{mut} - \Delta G^{wt} = \Delta\Delta G_{HP} + \Delta\Delta G_{conf} + \Delta\Delta G_{HB} + \Delta\Delta G_{cav} + \Delta\Delta G_{H_2O} + \Delta\Delta G_{pro}{}^{\alpha} + \Delta\Delta G_{pro}{}^{\beta} \quad (4)$$

where the hydrophobic term $\Delta\Delta G_{HP}$ can be defined as follows:

$$\Delta\Delta G_{HP} = 0.178\Delta\Delta ASA_{nonpolar} - 0.013\Delta\Delta ASA_{polar} \quad (5)$$

where $\Delta\Delta ASA_{nonpolar}$ and $\Delta\Delta ASA_{polar}$ represent the difference in ΔASA (accessible surface area) of nonpolar and polar atoms of all residues, respectively, between the wild-type and mutant proteins upon denaturation. For calculation of the ASA value, carbon and sulfur atoms in the residues are assigned to $ASA_{nonpolar}$ and nitrogen and oxygen atoms in the residues are assigned to ASA_{polar}. Parameters defining the contribution of these factors have been refined by a least-squares analysis of the structure−stability data derived from the analysis of the mutant protein relative to Gly ($\Delta\Delta G_{aa}$) (*43*). In the present case, the mutation site is completely buried in the interior of the molecule; therefore, the hydrophobic effect, conformational entropy, and secondary-structural propensity terms may be merged together and calculated relative to Gly ($\Delta\Delta G_{aa}{}^{\alpha} = \Delta\Delta G_{HP} + \Delta\Delta G_{conf} + \Delta\Delta G_{pro}{}^{\alpha}$) (*43*). Therefore, eq 4 can be written as follows:

$$\Delta\Delta G = \Delta\Delta G_{aa}{}^{\alpha} + \Delta\Delta G_{HB} + \Delta\Delta G_{cav} + \Delta\Delta G_{H_2O} \quad (6)$$

where

$$\Delta\Delta G_{H_2O} = -7.79\Delta N_{H_2O} \quad (7)$$

$$\Delta\Delta G_{cav} = -0.052\Delta V_{cav} \quad (8)$$

$$\Delta\Delta G_{HB} = 25.63\sum r_{[pp]}{}^{-1} + 15.62\sum r_{[pw]}{}^{-1} + 14.91\sum r_{[ww]}{}^{-1} \quad (9)$$

ΔN_{H_2O} and ΔV_{cav} are the changes in the number of water molecules and cavity volume ($\Delta V_{cav} = V_{cav}{}^{mut} - V_{cav}{}^{PCP-0SH}$) close to the mutation site, respectively. $r_{[pp]}$, $r_{[pw]}$, and $r_{[ww]}$ are the D::A distances for the protein−protein, protein−water, and water−water hydrogen bonds. In the case of the mutant proteins, no water−water hydrogen bonds were observed near position 192; however, one water molecule ($\Delta N_{H_2O} = 1$) was introduced in the cavity formed around position 192 in E192D and E192A mutant proteins. The parameters for $\Delta\Delta G_{H_2O}$ [−7.79 kJ mol^{-1} (water molecule)$^{-1}$], $\Delta\Delta G_{cav}$ (−0.052 kJ mol^{-1} Å^{-3}), and $\Delta\Delta G_{HB}$ (25.63 kJ Å mol^{-1} for intramolecular [pp], 15.62 kJ Å mol^{-1} for intermolecular [pw], and 14.91 kJ Å mol^{-1} for [ww] hydrogen bonds) have been determined by a least-squares fit of each $\Delta\Delta G$ (eq 4) to the experimental $\Delta\Delta G$ values using the high-resolution stability−structures database of the mutant human and T4 lysozyme (*21*). Equation 9 suggests that, if an intramolecular hydrogen bond of length 3.0 Å is removed by substitution, the mutant protein should be destabilized by 8.5 kJ/mol. The negative values of $\Delta\Delta G_{cav}$

Table 5: Structure-Based Empirical Stability of Monomeric PCP-0SH and E192 Mutant Proteins, Relative to the Putative Gly Mutant Protein

protein	$\Delta\Delta G_{aa}{}^{\alpha}$ [a]	$\Delta\Delta G_{HB}$ [b]	ΔV_{cav} [c]	$\Delta\Delta G_{cav}$	$\Delta\Delta G_{H_2O}$	$\Delta\Delta G$	$\Delta\Delta G^{mut-PCP-0SH}$ [d]
PCP-0SH	7.5	17.74	0.00	0.00		25.24	0.00
E192A	13.2	15.05	23.97	−1.25	−7.79	19.21	−6.03
E192D	6.3	22.62	13.48	−0.90	−7.79	20.23	−5.01
E192I	19.1		25.97	−1.35		17.75	−7.49
E192Q	5.4	16.92	0.00	0.00		22.32	−2.92
E192V	16.8		28.19	−1.47		15.33	−9.91

[a] The values for various residues have been taken from Takano and Yutani (*43*). All free-energy terms are defined in kJ/mol. [b] The hydrogen-bond energy because of water was calculated by using the three and four intermolecular hydrogen bonds in the case of E192A and E192D mutant proteins, respectively. [c] The change in cavity size ($\Delta V_{cav} = V_{cav}{}^{mut} - V_{cav}{}^{PCP-0SH}$) around position 192 was calculated using a probe radius of 1.1 Å. [d] $\Delta\Delta G^{mut-PCP-0SH}$ is the difference between $\Delta\Delta G$ values for the mutant proteins and PCP-0SH. The meaning of the other terms, $\Delta\Delta G_{aa}{}^{\alpha}$, $\Delta\Delta G_{HB}$, $\Delta\Delta G_{cav}$, $\Delta\Delta G_{H_2O}$, $\Delta\Delta G$, and ΔV_{cav}, has been described in the text.

and $\Delta\Delta G_{H_2O}$ terms suggest that the introduction of cavities and water in the protein structure leads to destabilization of proteins. An exhaustive least-squares analysis and evaluation of various parameters by taking into consideration a number of factors has been explained in detail by Funahashi et al. (*21*). A down point of these calculations, however, is that the analysis considers the denatured state to be a completely unfolded state, which in reality may not be always true (*32*). This assumption as well as uncertainty in coordinates in the high *B*-factor region, perhaps, leads to a standard deviation of up to 2.2 kJ/mol for data fitting on the experimental versus calculated $\Delta\Delta G$ values (*21*). Nevertheless, the analysis provides an important tool to evaluate the contribution of stabilizing factors to protein stability.

The hydrogen-bond length, *r*, for each type ($r_{[pp]}$, $r_{[pw]}$, and $r_{[ww]}$) in the case of each mutant was estimated from the crystal structures of the respective mutant protein. The change in the cavity volume because of the mutation was estimated by the procedure of Connolly (*44*) using the X-ray structures of the PCP-0SH and mutant proteins. In this study, the cavity volume around position 192 in PCP-0SH and mutant proteins was evaluated using a probe radius of 1.1 Å, because the cavity around position 192 upon removing the introduced water molecule in E192D and E192A structures was recognized when using a comparatively smaller probe radius of 1.1−1.2 Å.

The change in stability of each mutant with respect to PCP-0SH ($\Delta\Delta G^{mut-PCP-0SH}$) was evaluated from the difference in $\Delta\Delta G$ between the mutant and PCP-0SH. Table 5 lists the contribution of various factors to the stability of PCP-0SH and mutant proteins. The calculated structure-based $\Delta\Delta G$ values correlate well with the experimentally evaluated difference in the thermal stability (ΔT_d) and activation Gibbs energy ($\Delta\Delta G_u{}^{\ddagger H_2O}$) at low pH (Table 2), suggesting that refolding rates may be insensitive to substitution at position 192 at low pH. The results show that PCP-0SH is more stable than mutant proteins when E192 is protonated and forms two hydrogen bonds. Under these conditions, apolar mutant proteins show a lower stability than PCP-0SH (experimental $\Delta\Delta G_u{}^{\ddagger H_2O}$ and ΔT_d as well as calculated $\Delta\Delta G^{mut-PCP-0SH} < 0.0$). If E192 in PCP-0SH is assumed to be deprotonated, it cannot form any hydrogen bond and would thus decrease the relative PCP-0SH stability. This is also evident from the positive values of ΔT_d or $\Delta\Delta G_u{}^{\ddagger H_2O}$ for mutant proteins at alkaline pH (Figure 2 and Table 2), where PCP-0SH is less stable than other mutants. On the other hand, despite the large contribution of the $\Delta\Delta G_{aa}{}^{\alpha}$ term (mainly hydrophobic effects) to the stability of E192A, E192I, and E192V (Table 5), their empirical stabilities were less than PCP-0SH when E192 forms intramolecular hydrogen bonds (Figure 4A).

DISCUSSION

Electrostatic Stabilization of PCP-0SH. PCP-0SH from *P. furiosus* is an extremely thermostable protein, which denatures at above 105 °C at neutral pH (*30*). The denaturation temperature decreased to 59 °C at pH 2.15 (Table 1). The large shift in T_d by 46 °C because of the change in pH suggests a major contribution of electrostatic interactions. PCP-0SH is stabilized by complex network of salt bridges and hydrogen bonding, which are involved in intra- and intersubunit assembly and higher order oligomerization (*26*, *30*). The large decrease in PCP-0SH stability could be due to the dissociation of tetramer to dimer and monomer forms when pH decreases from the neutral to acidic region (*30*). An increase in the salt bridges and hydrogen bonding has been postulated to significantly contribute to the adaptation of proteins under extreme conditions (*3*−*6*). Although the role of salt bridges has been controversial because of the large desolvation penalty incurred over their formation (*8*, *9*), the reduced penalty at high temperature (*11*) and changes in the dielectric response of thermophilic proteins (*45*) result in a favorable contribution of salt bridges to the stability of folded proteins.

The pH-induced denaturation curves of PCP-0SH and the mutant proteins were highly cooperative and shifted to a high pH region for the mutant proteins relative to PCP-0SH (Figure 3). This suggests that the protonation−deprotonation of ionizable acidic groups, except for E192, is linked to the acid denaturation of the proteins, which is influenced by the residue at position 192. The relative stability of E192 mutant proteins increased in a nonparallel fashion with pH (Figure 2), and the fact that ΔT_d and $\Delta\Delta G_u{}^{\ddagger H_2O}$ values of the E192 mutant proteins change from negative to positive when pH increased suggests the important role of E192 in modulating the electrostatic interactions and hence the stability of PCP-0SH.

Glu192 in PCP-0SH Has an Apparently High pK_a. The crystal structure of PCP-0SH shows that the $O^{\epsilon 2}$ atom of E192 is very close to the backbone O (2.56 Å) and N (3.32 Å) atoms of P168 (Figure 4A). This could lead to a Coulombic repulsion if Glu $O^{\epsilon 2}$ is not protonated. A detailed structural analysis of proteins (*25*) has shown that a significantly large number of proteins contain at least one pair of carboxyl acids, which share a proton to form a short (∼2.55 Å) hydrogen bond. The E192 in PCP-0SH is completely surrounded by apolar groups. It has been observed

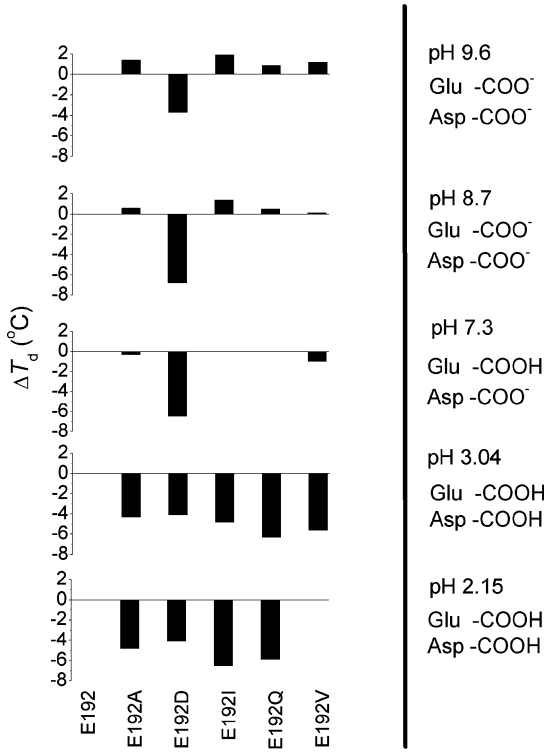

FIGURE 5: Relative stability (ΔT_d) of five mutants with respect to PCP-0SH at various pH values. The panel on right indicates the pH and predicted potonation−deprotonation status of the carboxyl groups in E192 and D192 based on stability as a function of pH.

that the hydrophobic environment (*46*−*48*) and proximity of the charged groups (*49*−*52*) can perturb the pK_a of ionizable groups. The protonation of Glu should reduce the electrostatic repulsion and promote forming hydrogen bonding as has been observed between the carboxyl and carboxylate groups (*25*, *53*).

The relative stability (ΔT_d) of the mutants compared to PCP-0SH changes from negative to positive; the transitions for E192 mutants were observed at pH 7.3 for E192Q and E192I, at pH 7.75 for E192A, and at pH 8.5 for E192V (Figure 2). The ΔT_d values of E192D, although always negative, were similar at pH values between 2.15 and 3.04, suggesting that Asp might be in the protonated state at low pH and hence less destabilizing. At higher pH, Asp begins deprotonating and hence more destabilizing because of the large energetic penalty incurred over charge burial. The relative stability of E192D decreases with the increasing pH to 7.3, while above pH 8.6, it sharply increases (Figure 2). In comparison to other polar and nonpolar mutants, E192D has a much lower stability in the neutral−alkaline pH zone, suggesting that a charged group is highly unfavorable at position 192. Figure 5 shows the relative stability of the E192 mutants and the possible status of the ionization of E192 and D192 based on the pH dependence of the stability. These results suggest that E192 might begin to deprotonate at pH $\geq$ 7, resulting in the breaking of the E192::P168 hydrogen bonds and concomitant lowering of the PCP-0SH stability. At pH $\geq$ 8.6, both E192 in PCP-0SH and D192 in E192D should be in a deprotonated and unfavorable state, resulting in the difference between the stabilities of these proteins becoming smaller. These results indicate that Glu is titrated between pH 7 and 9, while Asp may be titrated at a lower pH.

To verify the above results, we calculated the structure-based pK_a values of E192 and D192 carboxyl groups by the finite difference Poisson−Boltzmann (FDPB) procedure using the MEAD program (*54*, *55*). The FDPB calculates shifts in pK_a values from the pK_a of the model compound in solution (pK_{model}) because of three components viz., Born solvation energy of the charge group (ΔpK_{Born}), background energy of a charge with the nontitrating polar groups (ΔpK_{back}), and the interaction energy between the charge of interest and other titrating sites (ΔpK_{chrg}). The pK_a of a group in protein can thus be given as follows:

$$\mathrm{p}K_a^{\mathrm{protein}} = \mathrm{p}K_{\mathrm{model}} + \Delta\mathrm{p}K_{\mathrm{Born}} + \Delta\mathrm{p}K_{\mathrm{back}} + \Delta\mathrm{p}K_{\mathrm{chrg}} \quad (10)$$

The intrinsic pK_a (pK_{int}) is the pK_a of a titrating group considering that all of the other titrable groups are in the neutral form and can be written as follows:

$$\mathrm{p}K_{\mathrm{int}} = \mathrm{p}K_{\mathrm{model}} + \Delta\mathrm{p}K_{\mathrm{Born}} + \Delta\mathrm{p}K_{\mathrm{back}} \quad (11)$$

From eqs 10 and 11, we obtain

$$\mathrm{p}K_a^{\mathrm{protein}} = \mathrm{p}K_{\mathrm{int}} + \Delta\mathrm{p}K_{\mathrm{chrg}} \quad (12)$$

Using the pK_{model} values of 4.4 and 4.0 for Glu and Asp, respectively, their pK_a values were estimated to be 7.65 for E192 and 5.91 for D192, assuming a protein dielectric constant, ϵ_{pro}, of 15, because it has been suggested that for a static structure (single conformer) the FDPB procedures significantly improve the agreement between calculated and measured pK_a values at $\epsilon_{pro} = 10-20$ (*52*, *56*, *57*).

The calculated pK_a values of E192 and D192 are consistent with the pK_a values of the respective carboxyl groups predicted from the relative stabilities of E192 mutant proteins. The significantly higher pK_a values of E192 and D192 were originated partly from a contribution of the Born self-energy term ($\Delta\mathrm{p}K_{\mathrm{Born}}^{\mathrm{Glu}} = 2.4$ and $\Delta\mathrm{p}K_{\mathrm{Born}}^{\mathrm{Asp}} = 2.26$), which is indicative of the burial of the carboxyl group in the apolar environment (*52*, *55*, *56*). In the case of E192D, the presence of a water molecule close to D192 resulted in a significant decrease in the intrinsic pK_a of the carboxyl group because of a significant negative contribution from the background interactions ($\Delta\mathrm{p}K_{\mathrm{back}} = -2.13$), which almost fully compensated the pK_a upshift because of Born self-energy.

The titrating groups present in PCP-0SH also influenced the pK_a values of the buried carboxylic acids (E192 or D192) as shown by their higher pK_a values over their intrinsic pK_a ($\mathrm{p}K_{\mathrm{int}}^{\mathrm{Glu}} = 5.94$ and $\mathrm{p}K_{\mathrm{int}}^{\mathrm{Asp}} = 4.13$). The ΔpK_{chrg} values of 1.71 and 1.78 for E192 and D192, respectively, suggest unfavorable interactions of ionized carboxyl group at position 192 with other ionizable groups in the protein. PCP-0SH contains eight titrable acidic groups (D + E) within a radius of 15 Å from the residue 192. E192 or D192 have unfavorable pairwise interactions with the surrounding acidic groups. Therefore, to overcome the charge−charge repulsion, the equilibrium shifts toward the neutral carboxyl of E192 and D192. On the other hand, there are only four basic groups (K + R) within 15 Å from residue 192, which can favor the ionized acidic group at position 192. This means that E192 or D192 have much more repulsive interactions with acidic residues as compared to attractive interactions with basic

residues, resulting in a net pK_a shift to higher side. These results suggest that apart from the high self-energy because of charge burial the charge−charge interplay between E192 or D192 and charges at the surface or buried in the protein can affect PCP-0SH stability considerably. Recently, Makhatadze et al. (*12*) have shown that in addition to the short-range interactions long-range charge−charge interactions also play a crucial role in the stability of proteins. Several other studies have indicated significant influence of long-range charge−charge interactions on the pK_a of ionizable groups and the stability of proteins (*51*, *52*, *56*).

The buried E192 is surrounded by the proton acceptors rather than the donors in the hydrophobic pocket, resulting in the formation of favorable hydrogen bonds between the protonated carboxylic acid of E192 and the proton acceptors such as O and N atoms of P168. The strong hydrogen bonding should result in a further increase in the pK_a of the donor group of E192 (*49*) as has also been observed in the case of buried and hydrogen-bonded tyrosine residues (*52*, *58*). Several reports have shown the increases in the pK_a values of the carboxylic groups in the active site or buried location from 7.4 to 8.4 (*46*, *49*, *51*, *52*, *55*). Joshi et al. (*49*) have observed an apparently high pK_a ∼ 8.4 for Glu, leading to the formation of a strong hydrogen bond with an adjacent Asp in xylanase. Therefore, it seems that a large shift in the pK_a of ionizable groups is not rare and can take place to optimize the molecular interactions.

Buried Nonionized Glu Contributes More Than Polar and Hydrophobic Groups to PCP-0SH Stability. The calculated values of $\Delta\Delta G^{mut-PCP-0SH}$ (Table 5) indicate PCP-0SH to be more stable than the mutant proteins, which is consistent with the experimental stability monitored by DSC (Figure 2), denaturation kinetics (Table 2), and CD (Figure 3) measurements at low pH. A completely protonated Glu at low pH not only incurs a lower desolvation penalty but also acts as a strong hydrogen-bond donor. Also, a low dielectric constant environment of the buried E192 should result in a stronger hydrogen-bond formation in comparison to a similar one at the surface. On the other hand, the stabilities (T_d) of the PCP-0SH and E192Q/I/A mutant proteins were similar at pH 7.3, which was near the pK_a of E192 (Table 1). Therefore, assuming the stability of PCP-0SH is equal to the stabilities of the E192Q/I/A mutant proteins ($\Delta\Delta G$ in Table 5) and subtracting $\Delta\Delta G_{aa}^{\alpha}$ of PCP-0SH from the average $\Delta\Delta G$ of three mutant proteins, E192Q/I/A, the contribution of the hydrogen bonds ($\Delta\Delta G_{HB}$) by E192 for the putative Q/I/A → E mutations could be estimated to be 12.3 (±2.3) kJ/mol at pH 7.3. The reduced strength of the hydrogen bonds at pH ≥ 7.3 could be due to the partial deprotonation of E192, resulting in the partial rupture of the Glu::Pro interactions. In a case where the carboxyl group serves as a proton acceptor, the strength of the hydrogen bond decreases with a decrease in pH because of the protonation of the carboxyl group; however, in the present case, where carboxylic acid serves as a proton donor, the hydrogen bond should be stronger at low pH, unlike a carboxyl::amide hydrogen bond. The additional stability of PCP-0SH at low pH should originate from the strengthening of the hydrogen bonds made by E192, because $\Delta\Delta G_{aa}^{\alpha}$ should not change with pH. When E192 is deprotonated and the hydrogen bonds are broken, the $\Delta\Delta G$ of PCP-0SH decreases to 7.5 kJ/mol, which is essentially due to the $\Delta\Delta G_{aa}^{\alpha}$ term (hydrophobic effect) (Table 5) and consistent with the experimental results in the alkaline region, where mutants are more stable than PCP-0SH.

The side chain of Gln does not ionize, and hence, the strength of the GlnN$^{\epsilon}$::O═C (carbonyl oxygen of P168 and M187) hydrogen bond should not be significantly affected by a change in pH in the studied range. This suggests that the relative stability of E192Q with respect to other non-hydrogen-bond-forming mutant proteins should not change with pH. This is obvious from the fact that relative stabilities of E192Q and E192I were similar within the experimental errors in the studied pH range (Figures 2 and 3). The more or less equal stabilities of E192Q and E192I suggest that a better packing and introduction of two hydrogen bonds by Gln fully compensate for the desolvation of polar groups (side-chain amide) and loss of the hydrophobic effect (decrease in $\Delta\Delta G_{aa}^{\alpha}$) because of a putative I/V → Q mutation.

It has been proposed that the loss of packing interactions rather than a reduced hydrophobic interaction contributes to a greater extent to the decrease in protein stability caused by a destabilizing mutation (*59*). Substitution of E192 by Ala, Asp, Val, or Ile in PCP-0SH inserted cavities around position 192 (Table 5), leading to the loss of packing interactions. These results indicate that polar-group burial resulting in the formation of hydrogen bonds and polar interactions, together with improved packing interactions, is superior to the hydrophobic effects (because of Val, Ile, or Ala) in their contribution to protein stability as has also been recently observed by other workers (*22*, *59*).

Contribution of Structural Water Molecules to Protein Stability. The decrease in van der Waals interactions because of cavity formation and entropic losses because of inserted water lead to destabilization of proteins (*60*). It has been observed that an I → A mutation with unsolvated cavities can destabilize proteins by 12−14 kJ/mol (*19*). On the other hand, we observed that E192A is equally or more stable than E192I, E192V, and E192Q at acidic and alkaline pH values. The highly ordered state of water (B factor = 10 ± 4 Å^2) and the proximity with hydrogen-bond-forming partners in E192A/D implies that a water molecule can form several hydrogen bonds in the cavity (parts C and D of Figure 4). Table 5 lists the contribution of the intermolecular hydrogen bonding to the stability of E192A, which is consistent with the observed stability measured by DSC and CD at low pH. The relatively higher values of T_d at low pH on one hand and lower values of pH_{50} on the other hand for E192D and E192A in comparison to other mutant proteins suggest that intermolecular hydrogen bonds significantly contribute to the protein stability. Results shown in Table 5 indicate that the large enthalpic contribution by several protein−water hydrogen bonds not only offsets the water entropic loss but also stabilizes the E192A and E192D proteins by 6.0−13 kJ/mol (relative to empty cavities), assuming that the hydration effects of apolar and polar groups by entrapped water cancel each other (*61*). It has been observed that an entrapped water molecule significantly contributes to the protein stability (*17*, *19*, *20*) by forming 3−4 protein−water intermolecular hydrogen bonds (*62*) and improves van der Waals interactions by better packing (*63*).

Structural Basis for the Buried Glu192 Conserved in Hyperthermophilic PCPs. In the PCP-0SH monomer, E192

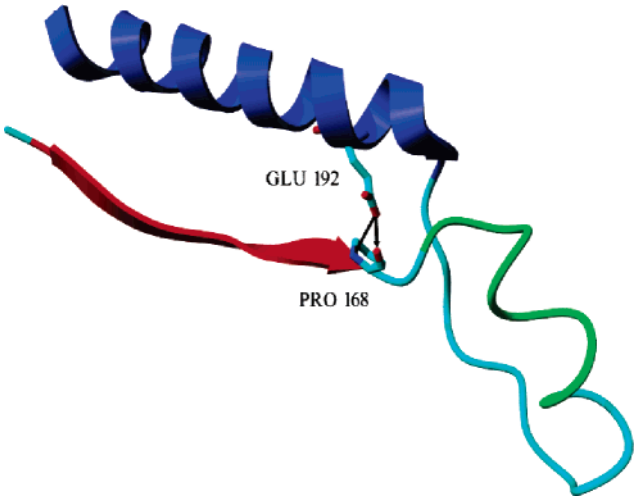

FIGURE 6: In the monomer structure of PCP-0SH, the loop (residues 169−188, colored cyan and green) connects the β strand (residues 161−167, colored red) with the α helix (189−208, colored blue). P168 and E192 are shown as sticks. The solid arrows indicate the atoms within the hydrogen-bond-forming distance.

is located at the beginning of a major α helix at the C terminal (residues 189−207) and spatially close to P168, which is located at the end of a β strand (residues 161−167) of a wide β sheet constituting the core of the PCP monomer. These secondary-structural elements are connected via a long flexible loop (residues 168−188) protruding out of the monomer structure (Figure 6). E192 projects toward P168 on the solvent-inaccessible side of the helix. The E192 $O^{\epsilon 2}$ and carbonyl O atom of P168 provide an excellent geometry to form a short tertiary hydrogen bond linking the α helix to the β strand. Strong hydrogen bonding between E192 and P168 restricts the helix to tear apart from the molecule and also stabilizes the intervening loop by raising the activation Gibbs energy of unfolding. Hydrogen bonds restricting the flexible loops play a critical role in maintaining the structural rigidity in proteins (*24*). Peterson et al. (*64*) have observed that a tertiary hydrogen bond between a helix and a β strand can stabilize a protein by 8.8 kJ/mol. A recent survey on 490 proteins belonging to different groups (*65*) indicates that the buried ionizable groups are more likely to be conserved than those on the surface and that the majority of the buried Glu can form two to three stabilizing interactions. The substitution of Glu to Ile, Val, Ala, or Asp in PCP-0SH resulted in the loss of packing interactions because of the creation of a cavity around position 192 (Table 5). Therefore, it seems that improved packing and strong hydrogen bonds formed between E192 and P168 could be responsible for the structural conservation of the glutamic acid buried in the interior of the hyperthermophiles proteins, in comparison to the other polar residues such as Asp or Gln or apolar residues such as Ala, Val, and Ile occupying the structurally corresponding position in the PCP from a mesophile, *B. amyloliquefaciens*.

CONCLUSION

The contribution of the Glu192 buried in the hydrophobic core in PCP-0SH and conserved in several hyperthermophilic PCPs to the protein conformational stability was examined using the mutations at position 192. The charged states of Glu and Asp at position 192 were unfavorable; however, their protonated forms were equally (D192 in E192D) or much more (E192 in PCP-0SH) stable below their pK_a values than even nonpolar substitutions (Ala, Ile, and Val) because of the involvement of their carboxylic acids in strong hydrogen bonding with the neighboring proton acceptors. Glu192 had an apparently high pK_a of ≥7.3, leading to the stability of PCP-0SH to be much higher (thermal stability change, $\Delta T_d \sim 4-6$ °C, and activation Gibbs energy change, $\Delta\Delta G_u^{\ddagger(H_2O)} \sim 7.4-12.3$ kJ/mol) than those of apolar mutants (E192A/I/V) at acidic pH, almost comparable to the stability of apolar mutants at neutral pH and the lower stability at alkaline pH. Glu192 has better packing than Asp, Ala, Ile, and Val in the hydrophobic pocket of PCP-0SH. The structural stabilization was mediated by a strong connection between an α helix (E192) and a β strand (P168) restricting a large flexible loop. Introduction of hydrogen bonding between protonated side-chain carboxyl and backbone carbonyl groups can be an attractive strategy to increase the protein stability at low pH, because, unlike carboxyl::amide hydrogen bonding, it becomes stronger with a decrease in pH. Intermolecular protein−water hydrogen bonds also significantly contribute to the protein stability. These facts may be taken into consideration for the rationale protein engineering and drug designing for increasing the binding or stability of proteins under extreme conditions.

ACKNOWLEDGMENT

We thank Dr. D. Bashford, Scripps Research Institute, CA, for his useful comments and generous help in running the MEAD program. We also thank Takara Bio, Inc., for providing PCP-0SH plasmid (pPCP3022).

REFERENCES

1. Rees, D. C. (2001) Crystallographic analyses of hyperthermophile proteins, *Methods Enzymol. 334*, 423−437.
2. Jaenicke, R., and Bohm, G. (2001) Thermostability of proteins from *Thermotoga maritima*, *Methods Enzymol. 334*, 438−469.
3. Vogt, G., Woell, S., and Argos, P. (1997) Protein thermal stability, hydrogen bonds, and ion pairs, *J. Mol. Biol. 269*, 631−643.
4. Kumar, S., Tsai, C. J., and Nussinov, R. (2000) Factors enhancing protein thermostability, *Protein Eng. 13*, 179−191.
5. Yip, K. S., Britton, K. L., Stillman, T. J., Lebbink, J., de Vos, W. M., Robb, F. T., Vetriani, C., Maeder, D., and Rice, D. W. (1998) Insights into the molecular basis of thermal stability from the analysis of ion-pair networks in the glutamate dehydrogenase family, *Eur. J. Biochem. 255*, 336−346.
6. Pappenberger, G., Schurig, H., and Jaenicke, R. (1997) Disruption of an ionic network leads to accelerated thermal denaturation of D-glyceraldehyde-3-phosphate dehydrogenase from the hyperthermophilic bacterium *Thermotoga maritima*, *J. Mol. Biol. 274*, 676−683.
7. Petsko, G. (2001) Structural basis of thermostability in hyperthermophilic proteins, or "There's more than one way to skin a cat", *Methods Enzymol. 334*, 469−478.
8. Honig, B., and Yang, A.-S. (1995) Free energy balance in protein folding, *Adv. Protein Chem. 46*, 27−58.
9. Waldburger, C. D., Schildbach, J. F., and Sauer, R. T. (1995) Are buried salt bridges important for protein stability and conformational specificity? *Nat. Struct. Biol. 2*, 122−128.
10. Anderson, D. E., Becktel, W. J., and Dahlquist, F. W. (1990) pH-induced denaturation of proteins: A single salt bridge contributes 3−5 kcal/mol to the free energy of folding of T4 lysozyme, *Biochemistry 29*, 2403−2408.
11. Elcock, A. H. (1998) The stability of salt bridges at high temperatures: Implications for hyperthermophilic proteins, *J. Mol. Biol. 284*, 489−502.
12. Makhatadze, G. I., Loladze, V. V., Ermolenko, D. N., Chen, X., and Thomas, S. T. (2003) Contribution of surface salt bridges to

protein stability: Guidelines for protein engineering, *J. Mol. Biol. 327*, 1135−1148.
13. Makhatadze, G. I., and Privalov, P. L. (1995) Energetics of protein structure, *Adv. Protein Chem. 47*, 307−425.
14. Myers, J. K., and Pace, C. N. (1996) Hydrogen bonding stabilizes globular proteins, *Biophys. J. 71*, 2033−2039.
15. Dill, K. A. (1990) Dominant forces in protein folding, *Biochemistry 29*, 7133−7155.
16. Campos, L. A., Cuesta-Lopez, S., Lopez-Llano, J., Falo, F., and Sancho, J. (2005) A double-deletion method to quantifying incremental binding energies in proteins from experiment: Example of a destabilizing hydrogen bonding pair, *Biophys. J. 88*, 1311−1321.
17. Takano, K., Yamagata, Y., Funahashi, J., Hioki, Y., Kuramitsu, S., and Yutani, K. (1999) Contribution of intra- and intermolecular hydrogen bonds to the conformational stability of human lysozyme, *Biochemistry 38*, 12698−12708.
18. Takano, K., Yamagata, Y., and Yutani, K. (2001) Contribution of polar groups in the interior of a protein to the conformational stability, *Biochemistry 40*, 4853−4858.
19. Takano, K., Yamagata, Y., and Yutani, K. (2003) Buried water molecules contribute to the conformational stability of a protein, *Protein Eng. 16*, 5−9.
20. Takano, K., Funahashi, J., Yamagata, Y., Fujii, S., and Yutani, K., (1997) Contribution of water molecules in the interior of a protein to the conformational stability, *J. Mol. Biol. 274*, 132−142.
21. Funahashi, J., Takano, K., and Yutani, K. (2001) Are the parameters of various stabilization factors estimated from mutant human lysozymes compatible with other proteins? *Protein Eng. 14*, 127−134.
22. Pace, C. N. (2001) Polar group burial contributes more to protein stability than nonpolar group burial, *Biochemistry 40*, 310−313.
23. Pace, C. N., Horn, G., Hebert, E. J., Bechert, J., Shaw, K., Urbanikova, L., Scholtz, J. M., and Sevcik, J. (2001) Tyrosine hydrogen bonds make a large contribution to protein stability, *J. Mol. Biol. 312*, 393−404.
24. Sinibaldi, F., Piro, M. C., Howes, B. D., Smulevich, G., Ascoli, F., and Santucci, R. (2003) Rupture of the hydrogen bond linking two Ω-loops induces the molten globule state at neutral pH in cytochrome *c*, *Biochemistry 42*, 7604−7610.
25. Wohlfahrt, G. (2005) Analysis of pH-dependent elements in proteins: Geometry and properties of pairs of hydrogen-bonded carboxylic acid side-chains, *Proteins 58*, 396−406.
26. Tanaka, H., Chinami, M., Mizushima, T., Ogasahara, K., Ota, M., Tsukihara, T., and Yutani, K. (2001) X-ray crystalline structures of pyrrolidone carboxyl peptidase from a hyperthermophile, *Pyrococcus furiosus*, and its Cys-free mutant, *J. Biochem. 130*, 107−118.
27. Singleton, M., Isupov, M., and Littlechild, J. (1999) X-ray structure of pyrrolidone carboxyl peptidase from the hyperthermophilic archaeon *Thermococcus litoralis*, *Struct. Fold. Des. 7*, 237−244.
28. Sokabe, M., Kawamura, T., Sakai, N., Yao, M., Watanabe, N., and Tanaka, I. (2002) The X-ray crystal structure of pyrrolidone-carboxylate peptidase from hyperthermophilic archaea *Pyrococcus horikoshii*, *J. Struct. Funct. Genomics 2*, 145−154.
29. Odagaki, Y., Hayashi, A., Okada. K., Hirotsu, K., Kabashima. T., Ito, K., Yoshimoto, T., Tsuru, D., Sato, M., and Clardy, J. (1999) The crystal structure of pyroglutamyl peptidase I from *Bacillus amyloliquefaciens* reveals a new structure for a cysteine protease, *Struct. Fold. Des. 7*, 399−411.
30. Ogasahara, K., Khechinashvili, N. N., Nakamura, M., Yoshimoto, T., and Yutani, K. (2001) Thermal stability of pyrrolidone carboxyl peptidases from the hyperthermophilic Archaeon, *Pyrococcus furiosus*, *Eur. J. Biochem. 268*, 3233−3242.
31. Ogasahara, K., Nakamura, M., Nakura, S., Tsunasawa, S., Kato, I., Yoshimoto, T., and Yutani, K. (1998) The unusually slow unfolding rate causes the high stability of pyrrolidone carboxyl peptidase from a hyperthermophile, *Pyrococcus furiosus*: Equilibrium and kinetic studies of guanidine hydrochloride-induced unfolding and refolding, *Biochemistry 37*, 17537−17544.
32. Kaushik, J. K., Ogasahara, K., and Yutani, K. (2002) The unusually slow relaxation kinetics of the folding-unfolding of pyrrolidone carboxyl peptidase from a hyperthermophile, *Pyrococcus furiosus*, *J. Mol. Biol. 316*, 991−1003.
33. Iimura, S., Yagi, H., Ogasahara, K., Akutsu, H., Noda, Y., Segawa, S., and Yutani, K. (2004) Unusually slow denaturation and refolding processes of pyrrolidone carboxyl peptidase from a hyperthermophile are highly cooperative: Real-time NMR studies, *Biochemistry 43*, 11906−11915.
34. Blaber, M., Zhang, X. J., and Matthews, B. W. (1993) Structural basis of amino acid α helix propensity, *Science 260*, 1637−1640.
35. Tiwari, A, Kumar, D. P., and Bhat, R. (2000) An efficient and cost-effective procedure for preparing samples for differential scanning calorimetry experiments, *Anal. Biochem. 284*, 406−408.
36. Otwinowski, Z., and Minor W. (1997) Processing of X-ray diffraction data collected in oscillation mode, *Methods Enzymol. 276*, 307−326.
37. Navaza, J., and Saludjian, P. (1997) AMoRe: An automated molecular replacement program package, *Methods Enzymol. 276*, 581−594.
38. Brunger, A. T., Adams, P. D., Clore, G. M., DeLano, W. L., Gros, P., Grosse-Kunstleve, R. W., Jiang, J. S., Kuszewski, J., Nilges, M., Pannu, N. S., et al. (1998) Crystallography and NMR system: A new software suite for macromolecular structure determination, *Acta Crystallogr., Sect. D: Biol. Crystallogr. 54*, 905−921.
39. Jones, T. A., Zou, J. Y., Cowan, S. W., and Kjeldgaard, M. (1991) Improved methods for building protein models in electron density maps and the location of errors in these models, *Acta Crystallogr., Sect. A: Found. Crystallogr. 47*, 110−119.
40. Laskowski, R. A., MacArthur, M. W., Moss, D. S., and Thornton, J. M. (1993) ProCheck-A program to check the stereochemical quality of protein structures, *J. Appl. Crystallogr. 26*, 283−291.
41. Jaenicke, R., and Bohm, G. (1998) The stability of proteins in extreme environments, *Curr. Opin. Struct. Biol. 8*, 738−748.
42. Kabsch, W., and Sander, C. (1983) Dictionary of protein secondary structure: Pattern recognition of hydrogen-bonded and geometrical features, *Biopolymers 22*, 2577−2637.
43. Takano, K., and Yutani, K. (2001) A new scale for side-chain contribution to protein stability based on the empirical stability analysis of mutant proteins, *Protein Eng. 14*, 525−528.
44. Connolly, M. L. (1993) The molecular surface package, *J. Mol. Graphics 11*, 139−141.
45. Dominy, B. N., Minoux, H., and Brooks, C. L., III (2004) An electrostatic basis for the stability of thermophilic proteins, *Proteins 57*, 128−141.
46. Yutani, K., Ogasahara, K., Aoki, K., Kakuno, T., and Sugino, Y. (1984) Effect of amino acid residues on conformational stability in eight mutant proteins variously substituted at a unique position of the tryptophan synthase α-subunit, *J. Biol. Chem. 259*, 14076−14081.
47. Smith, S. O., Smith, C. S., and Bormann, B. J. (1996) Strong hydrogen bonding interactions involving a buried glutamic acid in the transmembrane sequence of the neu/erbB-2 receptor, *Nat. Struct. Biol. 3*, 252−258.
48. Fukamizo, T., Juffer, A. H., Vogel, H. J., Honda, Y., Tremblay, H., Boucher, I., Neugebauer, W. A., and Brzezinski, R. (2000) Theoretical calculation of pK_a reveals an important role of Arg205 in the activity and stability of *Streptomyces* sp. N174 chitosanase, *J. Biol. Chem. 275*, 25633−25640.
49. Joshi, M. D., Sidhu, G., Pot, I., Brayer, G. D., Withers, S. G., and McIntosh, L. P. (2000) Hydrogen bonding and catalysis: A novel explanation for how a single amino acid substitution can change the pH optimum of a glycosidase, *J. Mol. Biol. 299*, 255−279.
50. Chen, H. A., Pfuhl, M., and Driscoll, P. C. (2002) The pH dependence of CD2 domain 1 self-association and ^{15}N chemical exchange broadening is correlated with the anomalous pK_a of Glu41, *Biochemistry 41*, 14680−14688.
51. Pace, C. N., Huyghues-Despointes, B. M., Briggs, J. M., Grimsley, G. R., and Scholtz, J. M. (2002) Charge−charge interactions are the primary determinants of the pK_a values of the ionizable groups in ribonuclease T1, *Biophys. Chem. 101−102*, 211−219.
52. Laurents, D. V., Huyghues-Despointes, B. M., Bruix, M., Thurlkill, R. L., Schell, D., Newsom, S., Grimsley, G. R., Shaw, K. L., Trevino, S., Rico, M., Briggs, J. M., Antosiewicz, J. M., Scholtz, J. M., and Pace, C. N. (2003) Charge−charge interactions are key determinants of the p*K* values of ionizable groups in ribonuclease *Sa* (pI = 3.5) and a basic variant (pI = 10.2), *J. Mol. Biol. 325*, 1077−1092.
53. Delbruck, H., Mueller, U., Perl, D., Schmid, F. X., and Heinemann, U. (2001) Crystal structures of mutant forms of the *Bacillus caldolyticus* cold shock protein differing in thermal stability, *J. Mol. Biol. 313*, 359−369.
54. Bashford, D., and Karplus, M. (1990) pK_a's of ionizable groups in proteins: Atomic detail from a continuum electrostatic model, *Biochemistry 29*, 10219−10225.

55. Dillet, V., Dyson, H. J., and Bashford, D. (1998) Calculations of electrostatic interactions and pK_as in the active site of *Escherichia coli* thioredoxin, *Biochemistry 37*, 10298−10306.
56. García-Moreno, E. B., and Fitch, C. (2004) Structural interpretation of pH and salt-dependent processes in proteins with computational methods, *Methods Enzymol. 380*, 20−51.
57. Fitch, C. A., Karp, D. A., Lee, K. K., Stites, W. E., Lattman, E. E., and García-Moreno, E. B. (2002) Experimental pK_a values of buried residues: Analysis with continuum methods and role of water penetration, *Biophys. J. 82*, 3289−3304.
58. Wilbur, D. J., and Allerhand, A. (1976) Titration behavior of individual tyrosine residues of myoglobins from sperm whale, horse, and red kangaroo, *J. Biol. Chem. 251*, 5187−5194.
59. Das, M., Rao, B. V., Ghosh, S., and Varadarajan, R. (2005) Attempts to delineate the relative contributions of changes in hydrophobicity and packing to changes in stability of ribonuclease *S* mutants, *Biochemistry 44*, 5923−5930.
60. Dunitz, J. D. (1994) The entropic cost of bound water in crystals and biomolecules, *Science 264*, 670.
61. Buckle, A. M., Cramer, P., and Fersht, A. R. (1996) Structural and energetic responses to cavity-creating mutations in hydrophobic cores: Observation of a buried water molecule and the hydrophilic nature of such hydrophobic cavities, *Biochemistry 35*, 4298−4305.
62. Hubbard, S. J., Gross, K.-H., and Argos, P. (1994) Intramolecular cavities in globular proteins, *Protein Eng. 7*, 613−626.
63. Wade R. C., Mazor, M. H., McCammon, J. A., and Quiocho, F. A. (1991) A molecular dynamics study of thermodynamic and structural aspects of the hydration of cavities in proteins, *Biopolymers 31*, 919−931.
64. Peterson, R. W., Nicholson, E. M., Thapar, R., Klevit, R. E., and Scholtz, J. M. (1999) Increased helix and protein stability through the introduction of a new tertiary hydrogen bond, *J. Mol. Biol. 286*, 1609−1619.
65. Kim, J., Mao, J., and Gunner, M. R. (2005) Are acidic and basic groups in buried proteins predicted to be ionized? *J. Mol. Biol. 348*, 1283−1298.

BI052610N